Author Manuscript

Magnetic Field Dynamics in MAAX Satellite's Circular Polar Orbit: A Magnetic Model Comparison

Sanjay Kumar and Mark B. Moldwin

[1]Department of Climate and Space Sciences and Engineering, University of Michigan, Ann Arbor, Michigan, USA

Key Points:

- Investigating the fidelity of empirical models in reproducing magnetic field variations observed by the Polar satellite at high altitudes.
- The Tsygenenko 01 model accurately predicts the magnetic field in Polar/MFE observations, outperforming T89, T96, and T04 models.
- The T01 model provides reliable magnetic field predictions for high-altitude circular polar orbits of MAAX, supporting future mission data.

Corresponding author: Sanjay Kumar, kumarsa@umich.edu

This is the author manuscript accepted for publication and has undergone full peer review but has not been through the copyediting, typesetting, pagination and proofreading process, which may lead to differences between this version and the Version of Record. Please cite this article as doi: 10.1029/2025JA033975.

This article is protected by copyright. All rights reserved.

Author Manuscript

Abstract

Motivated by the unique high-altitude polar orbit of the NASA Magnetosphere Auroral Asymmetry eXplorer (MAAX) mission and its Magnetometer Array Distributed on MAAX (MADMAAX), we examine the high-altitude magnetic field environment and its response to solar wind conditions. Using a dataset from the Polar satellite magnetometer, we investigate the variations in the external magnetic field along its highly elliptical orbit. To obtain the external magnetic field, we subtract the internal field, estimated using the IGRF-95 model, from the observed data. Additionally, we compare the Polar observations with four empirical magnetospheric magnetic field models (T89, T96, T01, and T04) along the satellites orbit. Our comparison of the observed external magnetic field with the modeled fields finds that the T01 model provides the most accurate predictions, even near the satellite's perigee, outperforming the other models (T89, T96, T04) for the dataset used. To extend our findings, we simulate an artificial circular polar orbit with a radius of 7 RE, matching the proposed MAAX mission trajectory, and calculate the magnetic field distribution along this orbit using the T01 model. The results demonstrate that the T01 model reliably approximates the magnetic field for such a high-altitude circular polar orbit, highlighting its utility for future mission planning. Our findings provide valuable insights into the dependence of the external magnetic field on solar wind conditions, offering a better understanding of geomagnetic variations in the high-altitude regions and supporting the design and data interpretation of future missions like MAAX.

Plain Language Summary

This study focuses on understanding the magnetic environment in high-altitude polar orbits, like the one planned for NASAs MAAX mission, as there are limited satellite observations in these regions. Using data from the Polar satellite magnetometer, we examined how the magnetic field changes along its elliptical orbit. We subtracted Earth's internal magnetic field using a model (IGRF-95) to focus on the external magnetic field. We used four Tsyganenko global magnetic field models to calculate the magnetic field along the orbit, considering concurrent solar wind parameters and other space weather factors. We found that the T01 model gave the most accurate results, even near the satellite's perigee, outperforming T89, T96, and T04. We simulated a circular orbit similar to NASA MAAX mission's path and used T01 to predict the magnetic field. Our results show that T01 provides a reliable estimate of the magnetic field in this orbit for planning future space missions like MAAX. Overall, our findings help us better understand the distribution of the magnetic field in high-altitude polar regions, which is important for understanding the connection between the magnetotail and the polar cap ionosphere and designing and interpreting data from future space missions.

1 Introduction

Earth has a robust intrinsic magnetic field, generated and sustained by the geodynamo process that occurs within its liquid outer core (Glatzmaiers & Roberts, 1995). Earth's intrinsic magnetic field extends into space, forming the magnetosphere, a dynamic region that serves as a protective barrier against the solar wind. This interaction between the solar wind and the magnetosphere deflects the majority of the charged particles carried by the solar wind. Nevertheless, some of these charged particles can penetrate the magnetosphere through magnetic reconnection on the dayside and propagate anti-sunward. When reconnection occurs again on the nightside, these particles are redirected toward Earth and become trapped along its closed magnetic field lines. Precise modeling of the near-Earth magnetic environment is crucial for understanding the dynamics of Sun-Earth connections, as the geomagnetic field governs fundamental processes in the geospace plasma, connecting the interplanetary medium with the ionosphere and upper atmosphere.

This article is protected by copyright. All rights reserved.

Author Manuscript

The magnetic field in the inner magnetosphere plays a crucial role in space weather predictions, as it significantly affects the behavior of charged particles and geomagnetic activity. Earth's magnetic field controls the movement of charged particles within the magnetosphere, and as these particles follow different trajectories, they generate various electric currents, including the ring current, tail current, and magnetopause currents (Ganushkina et al., 2015, 2018). These currents, in turn, play a crucial role in governing the dynamics of the magnetosphere, giving rise to phenomena such as geomagnetic storms and auroral activity.

Numerous satellites have measured magnetic fields in the magnetosphere, leading to the development of several useful magnetospheric magnetic field models (e.g., Olson and Pfitzer (1974); Mead and Fairfield (1975); N. A. Tsyganenko (1989); N. Tsyganenko (1996); N. A. Tsyganenko (2002b); N. A. Tsyganenko (2002a); N. A. Tsyganenko and Sitnov (2005) and others). Earlier studies of magnetospheric magnetic fields included the statistical analysis of the residual field ΔB, which represents the difference between the observed magnetic field and the Earth's internal field (Sugiura et al., 1971). That study, using data from the OGO-3 and OGO-5 spacecraft, presented findings of significant asymmetries between noon - midnight and dawn-dusk in ΔB, based on the categorization of the Kp index intervals. However, no attempt was undertaken to quantitatively correlate the field disturbance with solar wind conditions or the Dst index. Later, Fairfield et al. (1987) carried out a further statistical analysis of the near-Earth equatorial field using data from the Active Magnetospheric Particle Tracer Explorers (AMPTE)/CCE mission. Yet, the study only focused on the midnight region and did not describe the relationship between the observed magnetic field and other factors such as solar wind conditions or other geomagnetic indices. Instead, it simply grouped the data into a few intervals based on the Kp index. Iijima et al. (1990) studied the inner magnetospheric fields using data from the AMPTE and Combined Release and Radiation Effects satellites (CRRES) under disturbed conditions ($2 \leq Kp \leq 6$, and $-70 \leq Dst \leq -20$ nT). However, observations were limited to the equatorial regions, and the temporal coverage was relatively short. Nakabe et al. (1997) investigated the magnetic fields in the inner magnetosphere using data from Dynamic Explorer (DE) mission. Due to the orbital characteristics of DE-1, the magnetic field observations made by this spacecraft provided a unique data set to study the fields in the inner magnetosphere. DE-1 was a polar orbiting satellite and designed to observe the inner magnetosphere, with an apogee altitude of 3.63 RE, an inclination of 90 degrees and a 6.8-hour orbital period. The Polar satellite, launched in 1996, was designed to study Earth's auroras and the polar magnetosphere. The high precision of the Polar magnetometer allowed for accurate measurements of the external magnetic field, even near perigee. For more details on the Polar satellite, see Le and Russell (1998) and Zhou et al. (1997), along with the references therein, which examine the magnetic field dynamics over both low- and high-altitude polar caps using data from the Polar satellite. The study by N. A. Tsyganenko (1999) investigated the noon-midnight and dawn-dusk asymmetries in the external magnetic field in the near-Earth equatorial region, examining its dependence on solar wind dynamic pressure, SYM-H, and the interplanetary magnetic field (IMF). This analysis utilized data from the IMP 8, Wind, and Polar satellites.

However, due to the limited number of scientific satellites in high-altitude, polar orbits providing continuous coverage, the magnetic field structure in the inner magnetosphere over the high-latitude regions at geosynchronous altitudes has not been sufficiently studied.

To address this, the Magnetosphere Auroral Asymmetry eXplorer (MAAX) is a mission concept under NASA's Small Explorers program, designed to operate in a high-altitude circular polar orbit and provide a comprehensive view of the distortions and asymmetries in the aurora and magnetic field at both poles. MAAX consists of a pair of satellites, each equipped with ultraviolet cameras to capture images that fully cover the au-

This article is protected by copyright. All rights reserved.

Author Manuscript

roral ovals at both poles, as well as a Technology Demonstration Opportunity (TDO) Magnetometer Array Distributed on MAAX (MADMAAX) for magnetic field measurements. MADMAAX consists of four low size, weight and and power magneto-inductive magnetometers distributed on the spacecraft bus in combination with machine learning algorithms to enable high quality magnetic field measurements without the need of a boom (e.g., Regoli et al. (2018); Hoffmann and Moldwin (2024)).

By observing the auroral ovals in both hemispheres simultaneously, MAAX will enable a clearer understanding of the distortions and variations in the magnetic field that contribute to the generation of the aurora and the amount and time history of magnetic energy flow through the magnetosphere. In the first phase, the MAAX satellites are placed in polar orbits with an inclination of $\sim$ 90 degrees, at a distance of $\sim$ 7 RE, and spaced 90 degrees apart. This arrangement allows their cameras to capture the full extent of a single auroral oval, covering both the night and day sides of Earth. In the second phase, the satellites would be positioned 180 degrees apart in their polar orbits, enabling simultaneous imaging of auroras at both the North and South Poles. Simultaneous observations of auroral structures and asymmetries at both poles will provide essential data for magnetic mapping and deepen our understanding of magnetosphere-ionosphere coupling and auroral processes.

In this study, we focus on the variations in the external magnetic field along the MAAX satellite's orbit, which is a circular polar orbit with a radial distance of approximately 7 RE. High-altitude polar regions have a limited number of satellite observations; however, the Polar satellite has a highly elliptical polar orbit with a perigee of about 2 RE and an apogee around 9 RE. Therefore, we use magnetic field data from the Polar satellite for the year 1997 when its apogee was over the northern polar cap. We then calculate the magnetic field at Polar's locations using magnetospheric field models, such as the Tsyganenko models (1989, 1996, 2001, and 2004). By comparing the observed and calculated fields, we will determine which of these four models most accurately predicts the magnetic field observations over Polar's highly elliptical orbit. Finally, we modify the Polar orbit to a high-altitude circular polar orbit of radius 7 RE, similar to the MAAX trajectory, and apply the most accurate magnetic model to calculate the magnetic field at this orbit and analyze the dynamics of the magnetic field there. This paper is structured as follows: section 2 outlines the data selection and models used, section 3 presents the findings, and section 4 provides a discussion and conclusions of the results.

2 Data and models

The primary analysis utilizes data from the Magnetic Field Experiment (MFE) onboard the Polar satellite. The Polar spacecraft (1996-1999) follows a highly elliptical polar orbit, ranging from 1.8 to 9 RE in radius. Magnetic field measurements are provided by the MFE instrument (Russell et al., 1995). The investigation of the magnetic field using the MFE instrument onboard the Polar spacecraft has been thoroughly described by Le and Russell (1998) and references therein. During the processing of the original Polar MFE data, the observed magnetic field vectors were averaged to 1-minute intervals. The total number of data points, after averaging over 1 minute, is 517,844. The data were then visually inspected to identify and remove any erroneous measurements. The magnetic field data from MFE have been supplemented with the OMNI dataset (`https://omniweb.gsfc.nasa.gov/form/omni_min_def.html`), which provides solar wind and interplanetary magnetic field (IMF) measurements time-shifted to the Earth's bow shock for contextual analysis (King, 2005). The residual (external) magnetic field is determined by subtracting the International Geomagnetic Reference Field (IGRF-95) from the observed magnetic field. The most commonly used external magnetic field models for studying the Earth's magnetosphere and its response to solar wind dynamics are Mead and Fairfield (1975); Olson and Pfitzer (1974), and the Tsyganenko models (N. A. Tsyganenko (1989), T89; N. Tsyganenko (1996), T96; N. A. Tsyganenko (2002b, 2002a), T01

This article is protected by copyright. All rights reserved.

Author Manuscript

and N. A. Tsyganenko and Sitnov (2005), T04). These models provide a semi-empirical representation of the magnetospheric magnetic field.

The T89 model utilizes the Kp geomagnetic index as its primary input to assess the level of geomagnetic disturbance. The model was developed using data obtained from the Interplanetary Monitoring Platform (IMP) and the Highly Eccentric Orbit Satellite (HEOS) missions. The T96 model uses the upstream solar wind dynamic pressure, the IMF components By and Bz, the Dst index, and the dipole tilt angle as its input parameters. The magnetospheric magnetic field data utilized for this model include measurements from the Interplanetary Monitoring Platform (IMP), HEOS, and International Sun-Earth Explorer (ISEE) missions. The T01 model incorporates input parameters such as the solar wind dynamic pressure, Dst index, and the IMF By and Bz components, alongside two additional parameters, G1 and G2, which capture the temporal evolution of solar wind-magnetosphere interactions. This model relies on magnetic field data collected by the Polar, Geotail, ISEE, AMPTE, CRRES, and DE-1 satellites. The T01 model is similar to the T96 model but incorporates G1 and G2, which allow it to more effectively capture the time-dependent effects of solar wind driving on the magnetosphere. The T01 model incorporates data from high-altitude polar regions (from Polar), whereas earlier models were primarily based on equatorial data. The T04 model is parameterized by solar wind pressure, Dst, IMF By/Bz, and six parameters (W1W6), which represent the strengths of individual field sources. It also accounts for the non-linear saturation of these field sources under strong solar wind conditions, providing an accurate representation of the magnetosphere's behavior during intense solar wind driving. The magnetic field data set used to develop this model was obtained from observations by the GOES, Polar, Geotail, and Equator-S satellites. Additionally, the solar wind driving parameters G and W (Qin et al., 2007), utilized in the T01 and T04 models, were derived using the SpacePy Python package, available at `https://spacepy.github.io/index.html`. We utilize these models (T89-04) available through the Geopack Python library (`https://github.com/tssssss/geopack`) and compare them with external magnetic field data from the Polar satellite to identify which Tsyganenko model most accurately predicts the external magnetic field along the Polar satellite's orbit. The selected model is then used to forecast temporal variations of the magnetic field along the high-altitude circular polar orbit of MAAX.

The magnetic field data are provided in GSM coordinates, where the X-axis points from Earth toward the Sun, the Z-axis aligns with Earth's magnetic dipole, with its positive direction pointing toward the geomagnetic north pole, and the Y-axis is perpendicular to both the X and Z-axes, completing the right-handed coordinate system.

3 Results

For this study, we utilized data from the year 1997 collected by the Polar satellite, which follows a highly elliptical orbit with an inclination of 86 degrees. The spatial distribution of satellite data in the Y-Z plane is illustrated in Figure 1, with Earth at the center and the magnetopause boundary indicated by a black dashed curve. The satellite's orbit has an apogee of approximately 9 R_E and a perigee of 1.8 R_E.

During this time, the satellite's trajectory was primarily positioned over the northern polar region as shown in Figure 1. Although the validation was based on data from the northern polar region, the underlying models are designed to be approximately symmetric between geomagnetically conjugate locations. Therefore, similar performance is expected in the southern hemisphere under comparable solar wind and seasonal conditions. The number of observations is higher at the satellite's apogee, as shown in the figure, due to its slower speed, allowing for a greater number of measurements in that region. Magnetic field lines around Earth, obtained using the field line tracing method, are shown in the Figure 1. The field lines are traced using the Tsyganenko T89 model

This article is protected by copyright. All rights reserved.

Author Manuscript

from Python Geopack for the period of October 10-11, 1997, illustrating the structure of Earth's magnetosphere. The most intense geomagnetic storm of 1997, with a Dst of -130 nT, occurred on October 1011. This study period was chosen for analyzing variations in the external magnetic field along the Polar satellite's orbit (Figure 3.2-8) and for evaluating which Tsyganenko model provides the most accurate predictions under strong solar wind driving conditions. The most intense geomagnetic storm is expected to produce the largest variations in the external magnetic field, providing an opportunity to evaluate how well empirical models capture the storms impact on the estimated fields. For additional details on the Polar satellite and its instruments onboard, refer to (Le & Russell, 1998).

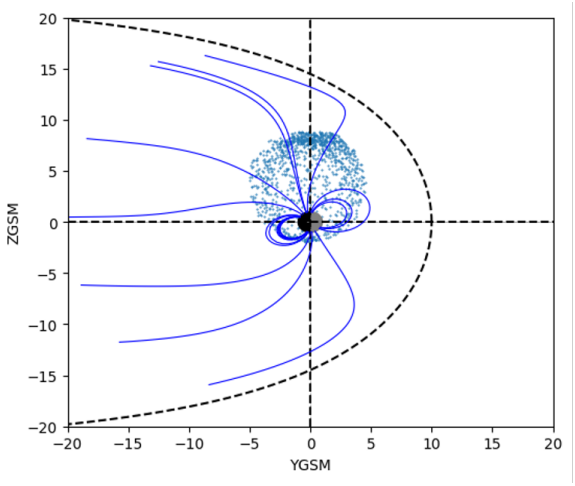


Figure 1. Spatial distribution of Polar satellite data in the Y-Z plane, with Earth at the center. The black dashed curve marks the magnetopause boundary. The data represents the Polar satellite's orbit, which reached an apogee of approximately 9 R_E, a perigee of 1.8 R_E. In 1997, the satellite's trajectory positioned it directly over the northern polar region. Magnetic field lines around Earth shown in the figure are obtained using the field line tracing method. The field lines are traced using the Tsyganenko T89 model from python Geopack for a specified time period (October 10-11, 1997), illustrating the structure of Earth's magnetosphere.

3.1 Residual vs. Modeled Field Comparison

Figure 2 (a−l) shows the statistical correlation between the residual external magnetic field and the magnetic field calculated using Tsyganenko models (T89,T96,T01,T04).

The residual and modeled magnetic field data are initially filtered to include only magnetic field directions within 25 degrees of the positive Z-axis, ensuring the selection of high-altitude data only ($Z > 5$ RE). After filtering, the data for each spacecraft passage (n=496) through this high-altitude polar region are averaged and plotted against each other, as shown in each panel of Figure 2.

Panels (a−c) illustrate the relationship between the different components of the residual magnetic field and those calculated using the T89 model. Each panel presents a scatterplot for the components B_x, B_y, and B_z, accompanied by their respective linear best-fit lines (solid black) and a reference line (dashed red) for comparison with a slope equal to one. The correlation coefficients and slopes of the best-fit lines, which quantify the strength and direction of the linear relationship, are displayed at the top of each

This article is protected by copyright. All rights reserved.

Author Manuscript

panel. The correlations were determined to be R = 0.51 for B_x, R = 0.57 for B_y, and R = 0.52 for B_z, indicating moderate positive correlations across all three components. Additionally, the slopes of the best-fit lines were 0.64, 0.69, and 0.39 for B_x, B_y and B_z, respectively. The data exhibit a scatter around the best-fit line, resulting in lower correlation coefficients for all the three components of B, with the largest scatter observed for B_z. The best-fit line represents the observed trend in the data, while the reference line with a slope of 1 serves as an idealized comparison. The differences between these lines highlight deviations between the observed and expected relationships, providing insight into the accuracy of the model and the extent of any systematic biases. This difference is most pronounced for the B_z component, where the maximum deviation occurs, indicating a greater departure from the expected linear trend for this particular magnetic field component. These slopes suggest that the modeled magnetic field components tend to underestimate the observed residual field, with varying degrees of agreement across the components. Overall, the results confirm a moderate quality of the residual data and calculated field and suggest using more advanced models or additional data sources to improve the accuracy of magnetic field predictions in the higher altitude regions.

Similarly to panels $(a{-}c)$, panels $(d{-}f)$ depict the relationship between the residual magnetic field components and those calculated using the T96 model. The correlation coefficients for B_x, B_y, and B_z were R=0.19, R=0.07, and R=0.20, respectively, indicating very weak positive correlations across all components. The slopes of the best-fit lines were 0.21 for B_x, 0.06 for B_y, and 0.11 for B_z, suggesting that the T96 model significantly underestimates the observed residual magnetic field. The difference between the best-fit line and the reference line further underscores the deviation between the observed and expected data across all magnetic field components, revealing a greater departure from the expected linear trend for each component. In this case as well, the data exhibit a scatter around the best-fit line, leading to lower correlation coefficients for all three components, with the largest scatter observed for B_x and B_z. These results demonstrate that the T96 model shows a weaker agreement with the observed residual magnetic field compared to the T89 model.

Next, we calculated the magnetic field using the T01 model, averaged it for each pass through the high-altitude region, and then plotted it against the residual magnetic field components, as shown in panels $(g{-}i)$. The correlation coefficients were determined to be R=0.88 for B_x, R=0.57 for B_y, and R=0.82 for B_z, reflecting a strong positive correlation for B_x and B_z and a moderate positive correlation for B_y. The slopes of the best-fit lines were 1.14 for B_x, 0.97 for B_y, and 1.06 for B_z, suggesting that the T01 model closely aligns with the observed residual magnetic field, with B_x and B_z slightly overestimated and B_y showing near-perfect agreement. The difference between the black line and the red dashed line also highlights the minimal deviation between the observed and expected data across almost all magnetic field components, revealing the best correlation for each component. These results highlight that the T01 model provides significantly better agreement with the observed residual magnetic field compared to both the T89 and T96 models.

Finally, we calculated the magnetic field using the T04 model and compared it with the residual magnetic field components. The correlation coefficients were found to be R=0.82 for B_x, R=0.56 for B_y and R=0.77 for B_z, indicating strong positive correlations for B_x and B_z, and a moderate positive correlation for B_y. The slopes of the best-fit lines were 0.90 for B_x, 0.60 for B_y, and 0.57 for B_z, suggesting that the T04 model provides a best-fit to the observed residual magnetic field, with varying degrees of underestimation across the components. One can notice a scatter around the best-fit line, with the most significant variation observed for B_z. The difference between the best-fit line and the reference line emphasizes the notable difference between the observed and expected data, particularly for the B_y and B_z magnetic field components, while showing the best correlation for B_x.

This article is protected by copyright. All rights reserved.

Author Manuscript

The T04 and T01 models provide the best match to the observed residual magnetic field data, with T01 offering the strongest overall agreement. While the T04 model also shows strong correlation with the residual magnetic field, it does not match the T01 model as closely in terms of accuracy. The T96 model, on the other hand, demonstrates poor correlation and is less effective in modeling the residual magnetic field. Overall, the T01 model stands out for its superior fit for the data used, making it the most reliable for magnetic field predictions in the high-altitude regions, while T04 offers a reasonable alternative, especially for certain components.

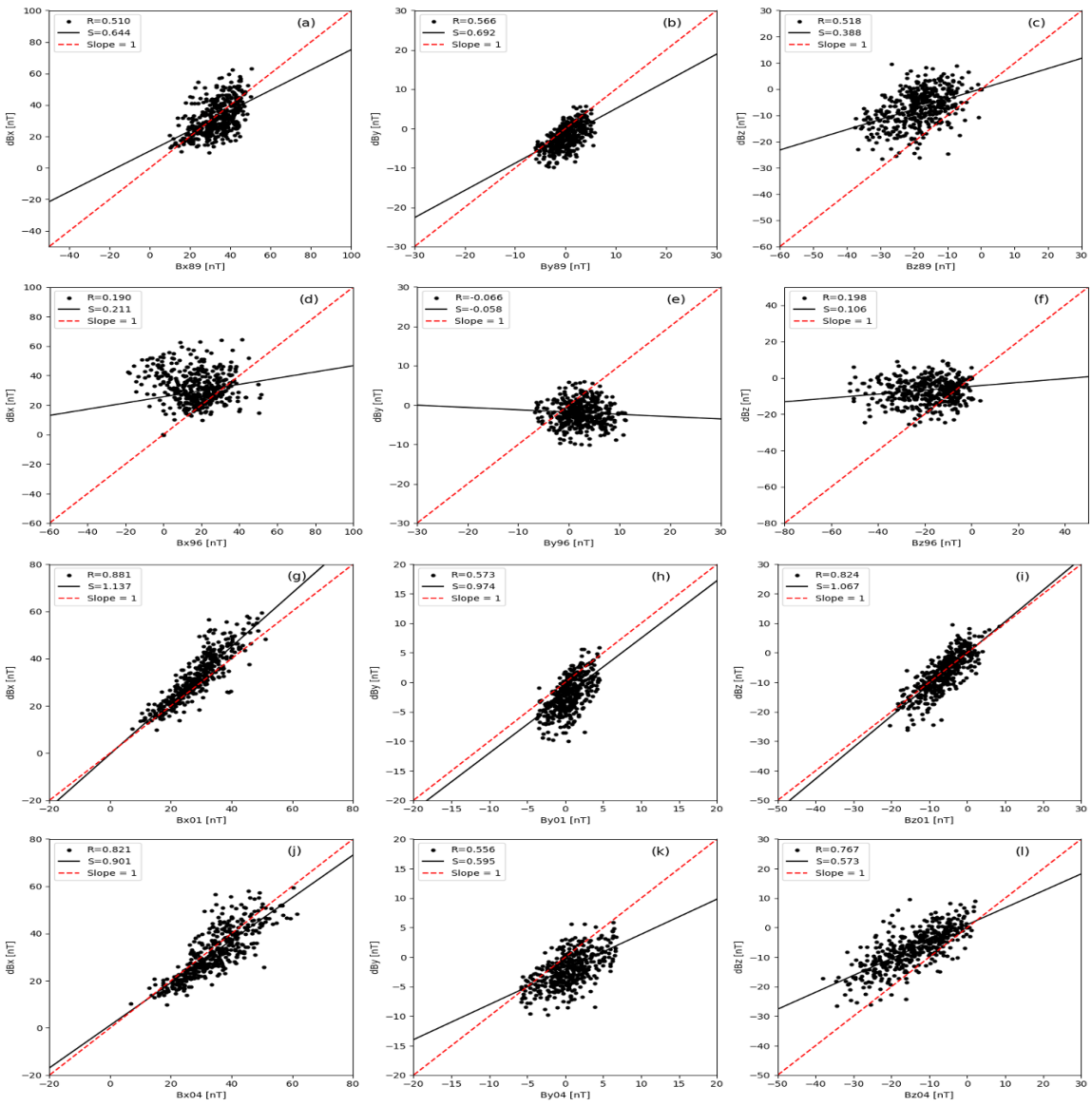


Figure 2. Panels (a-l) show scatter plots comparing the three magnetic field components calculated using the Tsyganenko 89-04 models with the residual magnetic field, dB ($B_{obs} - B_{IGRF}$), observed by the Polar spacecraft's MFE instrument over the entire year of 1997. In each panel, R represents the correlation coefficient, and S denotes the slope of the best-fit line (black) and a reference line (red dashed) with slope equal to one.

This article is protected by copyright. All rights reserved.

Author Manuscript

3.2 Magnetic Fields Variations

In this section, we plot the variation of the three GSM components of the magnetic field observed by Polar/MFE (red, green, purple) and magnetic field predicted by the T89-T04 models (blue) for October 10-11, 1997, to assess how well each model reproduces the residual field. All figures presented here display only the external component of the magnetic field, with the International Geomagnetic Reference Field (IGRF) subtracted from the observed data ($B_{x,y,x} - B_{IGRF}$ nT).

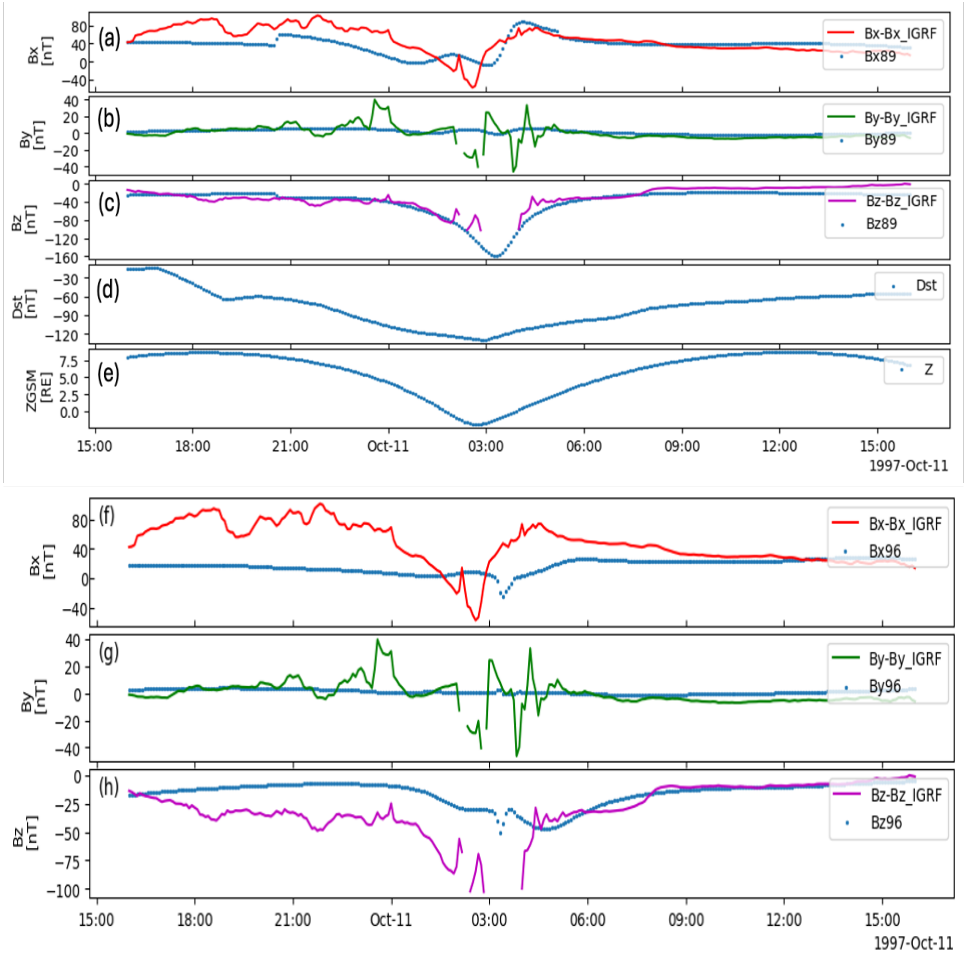
The upper panels (a–c) of Figure 3.2 show the components of the external magnetic field, represented by solid red (a), green (b), and purple (c) curves. The corresponding modeled field components, calculated using the T89 model, are overlaid as blue dotted lines in all the three panels (a, b, c). A data gap is evident in the Z component of the magnetic field (c). The cause of this gap is currently unclear; it may result from transmission issues, onboard anomalies, or ground-based data processing. Panel (d) displays the Dst index during this period, while panel (e) shows the Z GSM coordinate of the spacecraft's position. This time interval was chosen because it encompasses the strongest storm of 1997, which had a Dst of -130 nT at October 11, 3:00. This allows for the expectation of maximum variation in the external field and provides an opportunity to assess whether the empirical models capture the storm's response in the estimated fields. Variations in all field components are observed near the perigee, when the satellite is at $|Z| \sim$ 3 RE. Additionally, it is important to note that the peak of this storm occurred during this period, with a Dst of -130 nT. In the upper panels (a–c) of Figure 3.2 , the X component of the observed external magnetic field (red curve) varies between $\sim$ -60 and 100 nT, while the same component of the field modeled by T89 (blue dotted line) fluctuates between 0 and $\sim$ 80 nT. The difference between these two is clearly visible, particularly before the peak of the storm. However, after three hours of the peak, the observed and modeled fields align much more closely. The Y component of the observed field varies from $\sim$ -50 nT to 40 nT, while the modeled field fluctuates between $\sim$ -5 nT and 5 nT (panel b). There is a notable difference between the variations of both field components near the perigee and before that, but they align closely for the majority of the remaining period. The Z component (panel c), however, shows excellent agreement between the two curves throughout the entire period, including near the perigee, despite a data gap in that region of the orbit. Overall, these results suggest that the T89 model does not effectively capture the general trends of the external magnetic field, with significant variations remaining in the X and Y components.

To compare the differences between the observed and T96-modeled magnetic fields, we have plotted three magnetic field components in the lower panel of Figure 3.2 (f–h). The observed external field components exhibit same variations across upper and lower panels ($a - c$, $f - h$), whereas the modeled field components predicted by T96 model show distinct variations. The X component of the modeled field (blue dotted line) fluctuates between $\sim$ -30 and 20 nT. A significant difference between the residual and modeled field components is clearly visible, especially from the beginning until a few hours after the perigee. The Y component of the modeled field fluctuates between $\sim$ -5 nT and 5 nT (panel g). A noticeable difference is observed throughout most of the period. The component Z (panel h) varies between 0 to $\sim$ -50 nT (modeled). This component also exhibits a notable difference between the observed and modeled fields throughout the entire period, including near the perigee and for approximately two hours afterward. Therefore, similar to the T89 model, the T96 model does not accurately represent the general trends of the external magnetic field.

The upper panels (a–c) of Figure 3.2 show the comparison between the observed external magnetic field components and those predicted by the T01 model. The blue dotted line (modeled field) fluctuates between $\sim$ -130 and 100 nT (panel a). The difference between the two is minimal, with the exception of near the perigee. The Y component of the modeled field fluctuates between $\sim$ -40 nT and 5 nT (panel b). A noticeable dif-

This article is protected by copyright. All rights reserved.

Author Manuscript



Similarly, the lower panels ($f - h$) show the variation of the three GSM components of the observed external magnetic field (red, green, purple), while the blue dotted lines represent the field calculated using the T96 model for the same study period.

Figure 3. The upper panels ($a - c$) display the variation of the three GSM components of the magnetic field observed by Polar/MFE (red, green, purple) and predicted field calculated by the T89 model (blue dotted line) for October 10-11, 1997. Note that the International Geomagnetic Reference Field (IGRF) has been subtracted from the Polar data, and it is not included in the modeled field as well. Thus, the plots represent only the external component of the total field. Panels d and e show the Dst index and the Z-GSM coordinate along the Polar orbit during this period.
Similarly, the lower panels ($f - h$) show the variation of the three GSM components of the observed external magnetic field (red, green, purple), while the blue dotted lines represent the field calculated using the T96 model for the same study period.

ference is observed near and at the perigee. For the Z component (panel c), the modeled field fluctuates between 0 and $\sim$ -140 nT. Although there is only a small difference between the observed and modeled fields for most of the period, a more noticeable difference occurs at the perigee, where a data gap is also present in the observed field for this region. In contrast to the T89 and T96 models, the T01 model provides a much more

This article is protected by copyright. All rights reserved.

Author Manuscript

accurate representation of the external magnetic field, with only minor discrepancies observed at specific points.

The field components predicted by the T04 model and plotted alongside the observed ones are shown in the lower panels ($d-f$) of Figure 3.2. The variations in the X and Y components of the modeled fields closely resemble those predicted by the T01 model, as depicted in the upper panels (panels a and b). However, for the Z component (panel f), the modeled field fluctuates between -20 nT and $\sim$ -220 nT, showing a significant difference between the observed and modeled fields, particularly during three hours before and after the perigee. This model, like the T89 and T96 models, does not accurately predict the observed external field, but it provides better results in comparison to T89 and T96 models. Overall, among the four empirical models discussed, only the T01 model gives more accurate results than the others.

3.3 Field Differences

Figure 5 displays the differences between the observed external magnetic field components and the respective field components predicted by the T89, T96, T01, and T04 models for October 10 - 11, 1997 (panels $a-c$). These differences are used to evaluate the performance of each model in reproducing the observed magnetic field along the Polar satellite's orbit. The smallest differences between the observed and calculated field components suggest that the model offers a more accurate representation of the external magnetic field for the study period.

In Figure 5, the red solid curve represents the difference between the observed field and the field predicted by the T89 model. The other models are represented by color-coded dotted lines: The blue dotted curves represent the difference between the observed components and those predicted by the T96 model. Similarly, green for the T01 model, and black for the T04 model. This comparison highlights how well each empirical model replicates the observed field, offering valuable insights into the relative accuracy of the models.

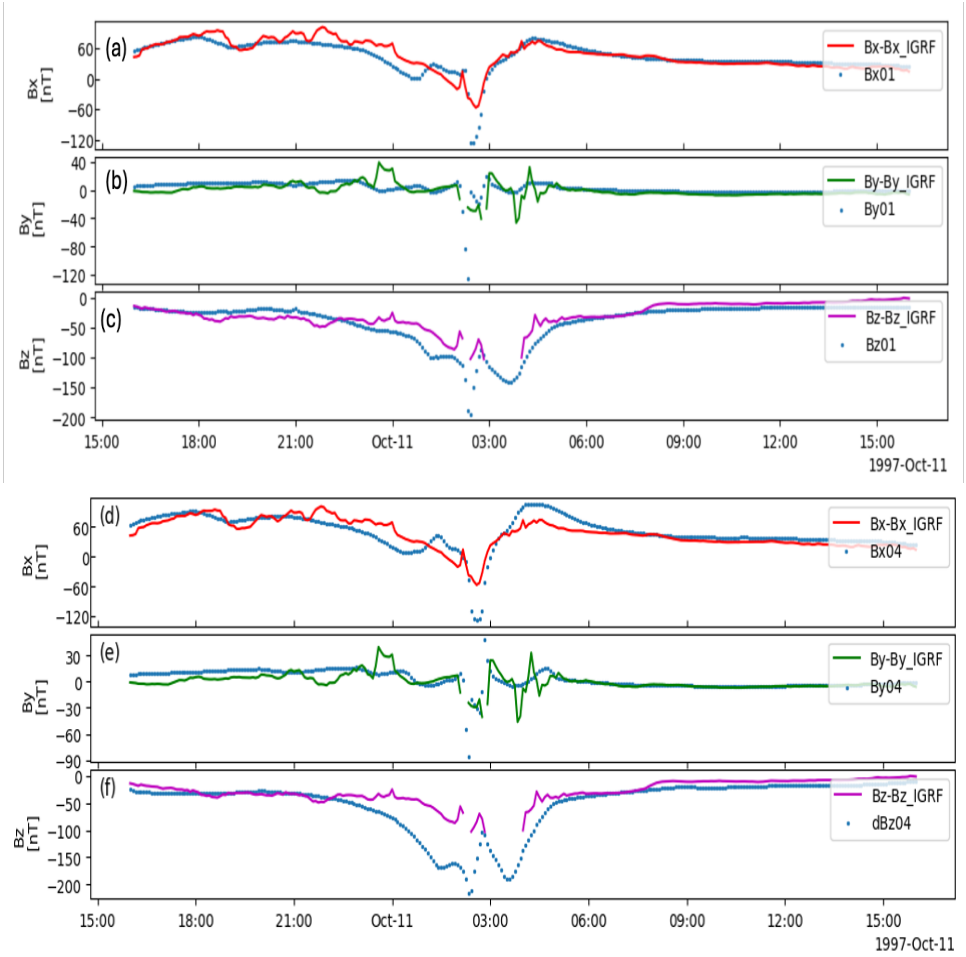
The difference between the X component of the observed and modeled magnetic field reveals noticeable variations across the different models. The T96 model (indicated by the blue dotted line) shows a significant difference, with the variation being larger compared to the T89 model (indicated by the red solid curve). The difference in the T89 model is somewhat smaller than that observed in the T96 model. On the other hand, the T01 model (represented by the green curve) shows the smallest differences, indicating a closer match with the observed field. The T04 model (black curve) exhibits differences similar to those of the T01 model, but with some wider variations in Z component near regions close to Earth (perigee) and during the late expansion and early recovery phases of the storm, suggesting that while it is relatively accurate, it is not as consistent as the T01 model.

The panel b displays the difference between the observed and modeled magnetic fields for the Y component, showing minimal variation across the different models, all of which closely match the observed field.

The difference in the Z component is shown in panel c, where variations in the difference values are observed across the models. For the T96 and T04 models, the difference between the observed and modeled fields is notably larger, particularly near the perigee. In contrast, the T89 and T01 models exhibit much smaller differences, with their predicted Z component values closely matching the observed data throughout the period, indicating better agreement for these two models. These results further confirm that all three components predicted by the T01 model are in very close agreement with the observed external magnetic field components.

This article is protected by copyright. All rights reserved.

Author Manuscript



In contrast, the lower panels ($d - f$) present the variations in the three components of the observed external magnetic field (red, green, purple), with the blue dotted lines showing the corresponding predictions made by the T04 model during the same time frame.

Figure 4. The upper panels ($a - c$) illustrate the variations in the three GSM components of the external magnetic field as observed by MFE instrument onboard Polar satellite (red, green, purple) and as predicted by the T01 model (blue dotted lines) for the period of October 10, 15:00, to October 11, 16:00, 1997.
In contrast, the lower panels ($d - f$) present the variations in the three components of the observed external magnetic field (red, green, purple), with the blue dotted lines showing the corresponding predictions made by the T04 model during the same time frame.

To clarify further, the panels (a–d) of Figure 3.3 display the differences between the total observed external magnetic field and the respective total fields predicted by the T89, T96, T01 and T04 models, represented by blue dotted curves, for the same study period. We filter the data for $R > 2$ RE ($R = (X^2 + Y^2 + Z^2)^{1/2}$) to exclude regions (near the perigee) where significant discrepancies are observed between the observed field and all the modeled fields as shown in Figures 3.2, 3.2, and 5. By examining these differences, we can identify which model provides the closest match to the observed external magnetic field.

This article is protected by copyright. All rights reserved.

Author Manuscript

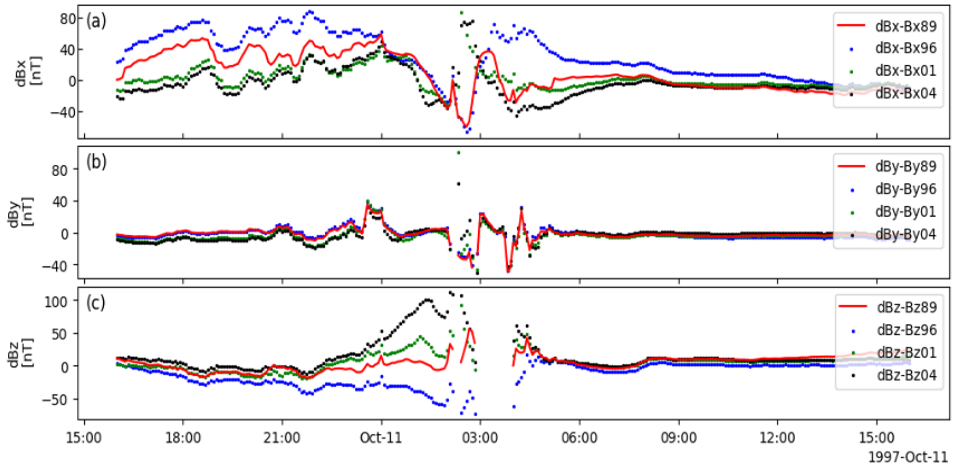


Figure 5. The panels $(a-c)$ show the differences between the observed external magnetic field components and the field components predicted by the T89, T96, and T04 models for the period of October 10, 15:00 to October 11, 16:00, 1997. The smallest differences between the observed and modeled fields indicate that one model may offer a more accurate representation than the others. In all panels (a-c), the red solid curve represents the difference between the observed field and the field predicted by the T89 model. The other dotted curves are color-coded as follows: Blue represents the difference between the observed field and the T96 model, Green represents the difference between the observed field and the T01 model, and Black represents the difference between the observed field and the T04 model.

Panel a depicts the difference between the total observed magnetic field and the total field predicted by the T89 model, with magnetic field values fluctuating between 4 and 67 nT. In panel b, the difference of the total observed field and the total field predicted by the T96 model is shown, varying from 6 to 98 nT. Panel c illustrates the difference between the total observed field and the modeled field from the T01 model, with values varying between 4 nT and 61 nT. Lastly, panel d presents the difference between the total observed and modeled magnetic fields using the T04 model, showing variations from 4 to 106 nT. The model that exhibits the smallest differences between its predicted field and the observed data is considered to offer a more accurate representation of the external magnetic field during the study period.

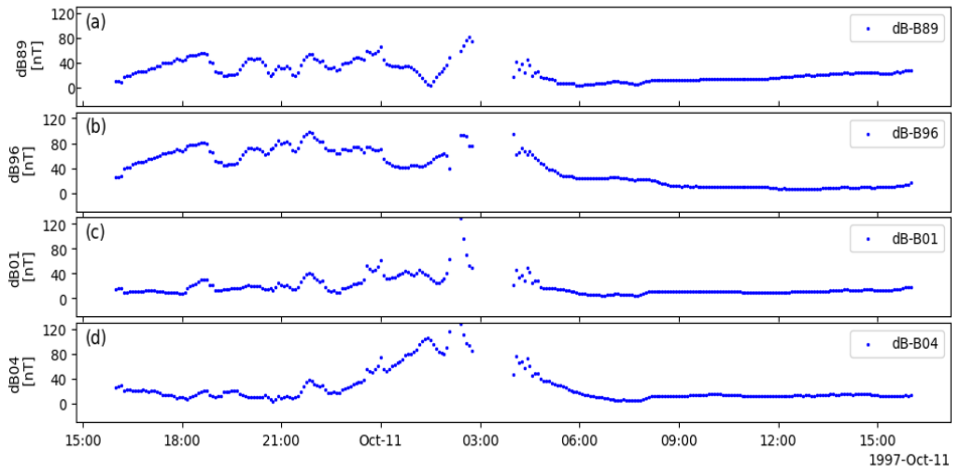
Based on the results presented in the panels $(a-d)$ of Figure 3.3, it is evident that the T01 model provides the smallest differences between the total observed external magnetic field and the predicted field, ranging from 4 to 61 nT. In comparison, the T89 and T96 models show slightly larger variations (panel a, b). The T04 model, although showing comparable performance to that of T01 model, exhibits a broader range of differences (4 to 106 nT) in panel d. Therefore, the T01 model is the most accurate in predicting the external magnetic field, as it shows the least deviation from the observed field across the study period.

3.4 MAAX orbit

To study the magnetic field dynamics at a circular polar orbit representing the MAAX satellite's trajectory, we created an artificial circular orbit with a radius of 7 RE. This was achieved by converting the elliptical orbit of the Polar satellite, which had an apogee of 9 RE and a perigee of $\sim$ 2 RE, into a circular orbit with a radius of 7 RE. Figure 7

This article is protected by copyright. All rights reserved.

Author Manuscript



The panels (a – d) display the differences between the total observed external magnetic field and the total field predicted by the T89, T96, T01 and T04 models for the period from October 10, 15:00 to October 11, 16:00, 1997. The model with the smallest differences between the observed and predicted fields suggests a more accurate representation.

Figure 6.

The panels (a – d) display the differences between the total observed external magnetic field and the total field predicted by the T89, T96, T01 and T04 models for the period from October 10, 15:00 to October 11, 16:00, 1997. The model with the smallest differences between the observed and predicted fields suggests a more accurate representation.

illustrates the spatial distribution of the artificial satellite's position data in the Y-Z plane, with Earth at the center and the magnetopause boundary marked by a black dashed curve. The satellite follows a circular orbit with a radius of 7 RE. The higher number of data points in the northern polar regions may result from the satellite spending more time in this area, similar to the Polar satellite's behavior (Figure 1). Similar to Figure 1, this figure also presents Earth's magnetic field lines generated with the field line tracing technique from Python Geopack for the October 1011, 1997, illustrating the structure of Earth's magnetosphere.

3.5 Magnetic field at the MAAX orbit

From Figures 2 to 3.3, we compare the IGRF-subtracted (external) magnetic field observed by the MFE instrument onboard the Polar satellite with the magnetic field predicted by four Tsyganenko models (T89-T04). The objective was to identify which empirical model best predicts the external magnetic field, closely matching the observed values. We found that, among the four models utilized, the T01 model predicted the magnetic field with great accuracy, closely matching the observed field for the data sets analyzed in this study. We now employ the T01 model to calculate the magnetic field dynamics along an artificially created circular polar orbit, representing the MAAX satellite's trajectory. The results are shown in the upper panels ($a-c$) of Figure 8 for the same period, October 10, 15:00 to October 11, 16:00, 1997.

The variation of the X component of B (B_X) along the circular orbit is shown in Figure 8 a, displaying values ranging approximately from $\sim$ -49 nT to 71 nT. The B_x component shows a significant increase from negative to positive values as the satellite moves along its orbit. A small variation is observed as the satellite transitions from one

This article is protected by copyright. All rights reserved.

Author Manuscript

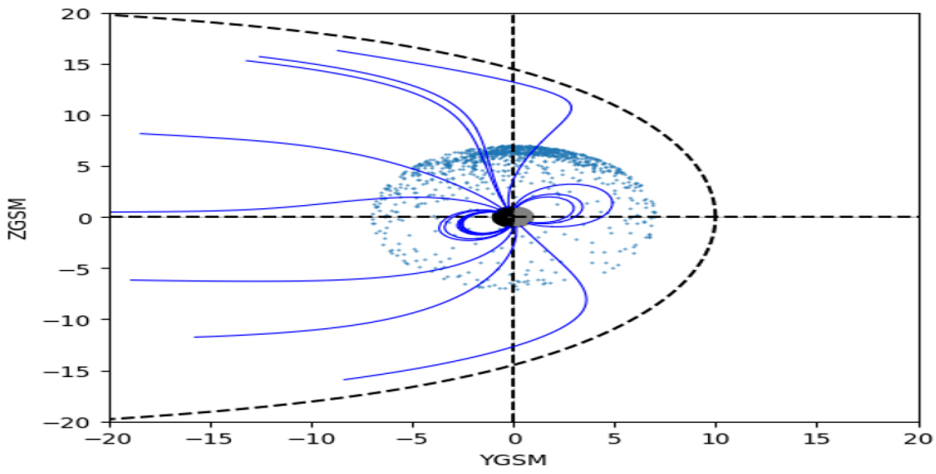


Figure 7. The spatial distribution of a simulated orbit data, representing the MAAX satellite trajectory, follows a circular polar orbit with a radius of 7 RE in the Y-Z plane, with Earth at the center. The black dashed curve indicates the magnetopause boundary. The figure displays Earth's magnetic field lines traced using the field line tracing method. These lines were generated with the Tsyganenko T89 model from Python Geopack for the specified period (October 1011, 1997), depicting the structure of Earth's magnetosphere.

hemisphere to another, crossing the magnetic equator (X-axis) near the marked red crosses. The two red crosses indicate the times when the satellite crosses the X-axis, as shown in the lower panel, where the B_X component is expected to be zero or near zero. The observed sign change in B_x suggests that the satellite is moving through different magnetospheric regions. As B_x changes from positive to zero (at the first red cross mark), it indicates the satellite crossing the X-axis from the northern hemispehere to the southern hemisphere. When B_x turns negative, the satellite moves into the southern hemisphere, returning to zero (at the second red cross mark) and then positive again, completing the cycle. This pattern can occur in both highly elliptical and circular polar orbits, as the satellites traverse the X-axis.

The lower panel of Figure 8 confirms this behavior of B_x through the satellite's motion (clockwise) as it moves from the northern hemisphere to the southern hemisphere (indicated by the red cross mark on the right), where B_x is zero. It then proceeds into the southern hemisphere, where B_x becomes negative. Afterward, B_x returns to zero (left red cross mark) as the satellite moves back towards the northern hemisphere. However, it is important to note that significant variations in B_x are observed prior to the peak of the geomagnetic storm (October 11, 03:00), which corresponds to the main phase of the storm, as indicated in the upper panel *d* of Figure 3.2. The main phase of the storm could likely be the primary cause of the significant changes observed in the X component of the magnetic field. The variation in the Y component (panel *b*) ranges from approximately -18 to 35 nT, occurring primarily during the main phase of the storm. The B_Y component initially rises to positive values before gradually decreasing. This behavior suggests changes in the east-west magnetic field component, potentially linked to the satellite's movement across different magnetic regions. After the main phase of the storm, the fluctuations subside and the field stabilizes at a nearly constant value of around 10 nT. Panel *c* illustrates the variation in the Z component of the modeled magnetic field (B_z), with decrease in B_z occurring around the same time as those observed in the X and Y components (panels *a* and *b*). The Z component varies between $\sim$ -43 and 14 nT,

This article is protected by copyright. All rights reserved.

Author Manuscript

with the primary cause of these significant changes likely being the geomagnetic storm and the satellite's passage from the northern hemisphere to the southern hemisphere and back to the northern hemisphere again (see the lower panel of Figure 8). The B_Z component exhibits a distinct pattern, starting with negative values, rising to zero, decreasing and then stabilizing. This variation is influenced by the satellite's movement across the north-south magnetic field structure.

To assess whether the changes in the magnetic field components shown in the upper panel (Figure 8 $a-c$) predicted by the T01 model are driven by the geomagnetic storm, we examined the same components during a quiet period ($Dst > -40$ nT). The results, presented in the panels ($a-c$) of Figure 9, correspond to the quiet interval from October 15 to October 16. In panel a, the X component of B varies between -29 nT and 21 nT, significantly lower compared to the storm-time variation shown in the upper panel a of Figure 8. Although, the Y component in Figure 9 b ranges from -15 to 12 nT, which is surprisingly higher than the storm-time variation of the same component (Figure 8 b). Likewise, the Z component in the lower panel c varies between -18 and 18 nT, showing a smaller fluctuation compared to its storm-time counterpart. By comparing the magnetic field components in Figure 8 ($a-c$) and Figure 9 ($a-c$), it is evident that the pronounced changes observed in ($a-c$) panel of Figure 8 are attributable to the geomagnetic storm. The variation in magnetic field components is primarily influenced by geomagnetic effects (such as storms), with a slight change occurring due to the satellite's passage from one hemisphere to another.

4 Discussion and Conclusions

Figure 2 presents scatter plots comparing the IGRF-subtracted (external) magnetic field components observed by Polar/MFE from January 1, 1997, to December 31, 1997, with the magnetic field components predicted by commonly used magnetospheric models (T89, T96, T01, T04). The predictions were generated using concurrent solar wind, IMF, and Dst data as input parameters for the same study period. The correlation coefficients (R) indicate moderate positive correlations across all three components for T89 model. Furthermore, the slopes (S) suggest that the modeled magnetic field components generally underestimate the observed residual field, with varying levels of agreement among the components. These findings confirm a moderate level of consistency between the residual data and the calculated magnetic field (T89). The comparison between the residual magnetic field components and those calculated using the T96 model shows very weak positive correlations across all components. The slopes of the best-fit lines indicate that the T96 model significantly underestimates the observed residual magnetic field, demonstrating even weaker agreement compared to the T89 model. N. A. Tsyganenko (2002a) analyzed the correlation between the observed external magnetic field from the DE-1 observations and the corresponding values predicted by the T96 model through scatter plots. The correlation coefficients (R) and slopes of the best-fit lines for these scatter plots were generally low across all components. However, both the correlation coefficients and the slopes were higher than those obtained in the current study when comparing the T96 model with Polar data.

The moderate correlation for the T89 model and weaker correlation for the T96 model between the observed external and modeled fields can be explained by the fact that these models were not based on observed data from the Polar satellite, these models were developed using data from the IMP, HEOS, and ISEE missions. Another reason for the very poor correlation for the T96 model could be attributed to the fact that this model performs best when the input parameters fall within specific ranges: solar wind dynamic pressure between 0.5 and 10 nPa, Dst between -100 and +20, and IMF components (By and Bz) between -10 and +10 nT (Le and Russell (1998)).

This article is protected by copyright. All rights reserved.

Author Manuscript

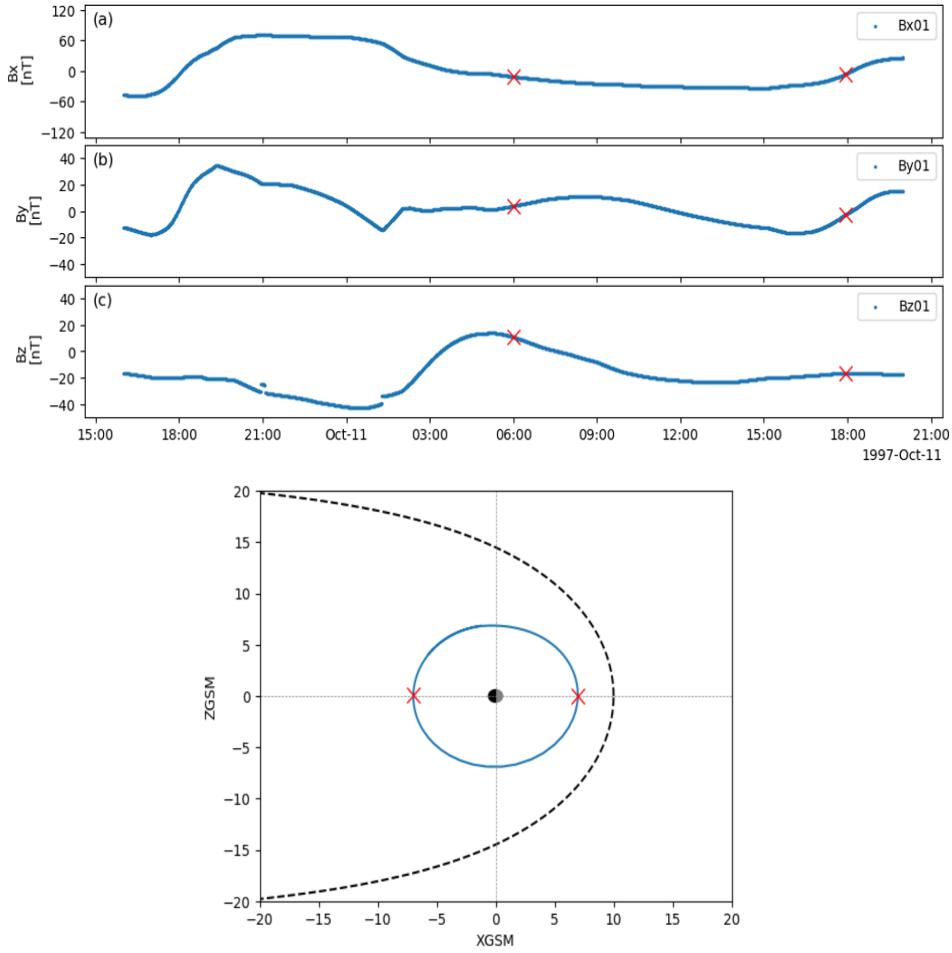


Figure 8. The panel (a – c) displays the magnetic field components predicted by the most accurate model for the current analysis, the T01 model, for the period from October 10, 15:00 to October 11, 16:00, 1997. The predicted field is calculated along the MAAX satellite's orbit (radius 7 RE). The two red cross marks displayed in all panels represent the corresponding times when satellite cross X-axis shown in the lower panel. The lower panel depicts the path of the satellite for the same period of October 10-11, 1997 as in upper panel. As the satellite moves clockwise, the points where it enters and exits the plasma sheet are indicated by red crosses.

The magnetic field calculated using the T01 model was plotted against the residual magnetic field components, as shown in panels (gi) of Figure 2. The correlation coefficients indicate a strong positive correlation. The slopes of the best-fit lines also suggest that the T01 model closely aligns with the observed residual magnetic field, highlighting that it provides significantly better agreement compared to both the T89 and T96 models. The magnetic field calculated using the T04 model was compared with the residual magnetic field components (panels (jl) of Figure 2), showing strong positive correlations based on the correlation coefficients. The slopes of the best-fit lines also indicate that the T04 model provides a good fit to the observed residual magnetic field. Although, both the T04 and T01 models offer the best match to the observed residual magnetic field data, the T01 model demonstrates the strongest overall agreement between the two. The strong positive correlations between the observed and modeled fields from these two models can be attributed to the fact that both models were developed using

This article is protected by copyright. All rights reserved.

Author Manuscript

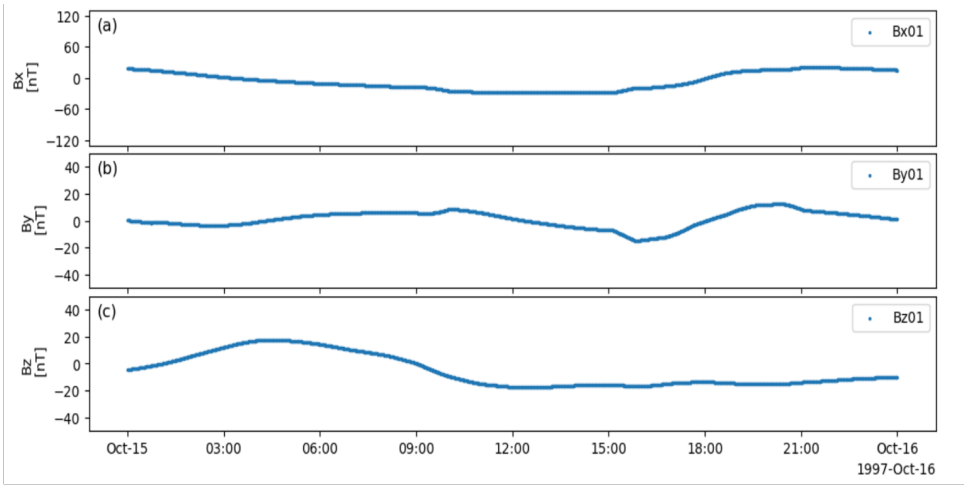


Figure 9. The panels $(a - c)$ depict the magnetic field components during a quiet period from October 15, 03:00, to October 16, 1997.

observed data from the Polar satellite. However, it is somewhat surprising that the T01 model provides a better correlation than the more advanced T04 model indicating that the T04 model does not capture the storm currents accurately at high latitudes in the polar cap even though the model was developed to better capture storm dynamics.

To further evaluate the accuracy of each model in reproducing the residual field, we compared the observed external magnetic field components with the modeled fields along the Polar satellite's orbit, as illustrated in Figures 3.2 and 3.2. Both the upper and lower panels $(a-c)$ of Figure 3.2 reveal that the fields modeled by the T89 and T96 models show poor agreement with the observed external field, with the T96 model performs more poorly. These findings are consistent with the results presented in Figure 2.

N. A. Tsyganenko (2002a) also examined the comparison between the three components of the field measured by the Polar satellite and the field predicted by the T96 model for a moderate Dst index (ranging from -15 nT to -60 nT). They found that the T96 model significantly overestimated each component, particularly near the perigees. In both instances (Dst:-15 nT to -60 nT), the T96 model predicted a much weaker field than was actually observed. Their results are consistent with those presented in this study (which covers all Dst values) shown here for the T96 model in the lower panel of Figure 3.2.

Figure 3.2 demonstrates that the fields predicted by both the T01 and T04 models align much more closely with the observed field compared to the T89 and T96 models. However, the T01 model performs better overall, as the T04 model does not predict the Z component as accurately specifically near the satellite perigee. Following the results presented in the scatter plot in Figure 2, the figures showing the magnetic field along the Polar orbit (Figures 3.2 and 3.2) further confirm that, among the four models used in this study, the T01 model provides the most accurate representation of the external magnetic field for the given dataset and study period. Next, we analyze the differences between the external magnetic field components and the corresponding modeled field components, as well as the difference between the total observed field and total modeled field, as shown in Figure 5 and 3.3, respectively. These comparisons further validate the results presented in Figures 2 and 3.2-3.2. The difference figures confirm that the differences between the observed field components and those predicted by the T01 model are the smallest. This again indicates that the T01 model produces results that closely match

This article is protected by copyright. All rights reserved.

Author Manuscript

the magnetic field measurements observed by the Polar magnetometer. Similarly, the minimal difference between the total observed field and the T01 model field underscores the better accuracy of the T01 model compared to the other models.

The agreement with Nishimura et al. (2011), who investigated the footprints of the THEMIS spacecraft in auroral regions using Tsyganenko models (T89, T96, T01, and T04) and validated T01 with 13 events of conjugate THEMIS spacecraft and ground-based imager measurements, underscores its efficacy for auroral mapping. They found that T01 provides reasonable footprint estimates, with deviations within 1-2 magnetic latitude (MLAT) and 0.1-0.2 hours magnetic local time (MLT), aligning with our polar data accuracy at 7 RE. Statistically, T01 outperformed T89 and T96, a finding consistent with our results from Polar data, highlighting its superiority in both auroral and polar contexts. Their model tends to overestimate field-line stretching during quiet geomagnetic conditions but performs well or underestimates stretching during active times, with MLT generally well-represented. This enhanced performance is likely due to T01s incorporation of more realistic current distributions and its reliance on preceding solar wind parameters, which better capture dynamic magnetospheric conditions. In contrast, T04, optimized for storm-time magnetic field modeling, may not accurately reproduce the field during non-storm times, a limitation that underscores T01s broader applicability across varying conditions. Although Nishimura et al. (2011)s analysis is limited to the proton aurora occurrence region near the equatorward auroral oval boundary, our study extends this by leveraging high-altitude Polar data, where T01s G1/G2 parameters and empirical adjustments enhance its representation of field asymmetries. This dual effectiveness supports T01s suitability for the MAAX missions circular polar orbit, enhancing its utility for magnetosphere-ionosphere coupling studies.

The T01 model was found to be the most accurate among T89, T96, and T04 when using standard model input parameters. This finding is somewhat unexpected, as more recent models like T04 and T07 would generally be expected to outperform older models (Brito and Morley (2017)). The superior performance of the T01 model over the T04 model could be attributed to its ability to better accommodate extreme solar wind and geomagnetic conditions, potentially leading to more accurate predictions during intense space weather events. Additionally, the T01 model's realistic current distributions, adaptability to varying geomagnetic conditions, and superior statistical performance could contribute to its reliability. These characteristics suggest that the T01 model may be more effective for modeling geomagnetic fields under challenging space weather conditions, especially for the datasets and the period of study used in this research. Our results differ from those of Le and Russell (1998) in few key aspects. While they focused solely on the T96 model and analyzed the magnetic field during the perigee pass of the Polar satellite, we expanded our comparison to include multiple Tsyganenko models (T89, T96, T01, and T04) and examined the magnetic field across the entire orbit of the spacecraft. This broader scope allows for a more comprehensive assessment of the models performance in various regions of the orbit, rather than being limited to the perigee. Additionally, while Le and Russell (1998) used fixed solar wind parameters from the Wind spacecraft, our analysis incorporates concurrent solar wind , IMF, and the Dst index as input conditions, providing a more robust comparison of the models across different orbital phases. In another study, Zhou et al. (1997) compared the magnetic fields observed at high altitudes above the polar cap by the Polar spacecraft with those predicted by the T96 model. They found that the magnetic field near the polar cusps was generally weaker than predicted by the T96 model. While their study focused on high-altitude regions near the polar cusps, our analysis extends to a wider range of orbital regions and compares multiple Tsyganenko models (T89, T96, T01, and T04). However, similar to their findings, our results also indicate that the T96 model did not provide accurate predictions when compared to the observed Polar data.

This article is protected by copyright. All rights reserved.

Author Manuscript

The superior performance of T01 in this study could be attributed to the absence of extreme storm-time dynamics, where T04 typically excels. T01s balance of complexity and responsiveness to moderate disturbances could align better with the current data. Additionally, the spatial and temporal scope of this study may correspond more closely with the regions and conditions T01 was designed to model, such as the inner magnetosphere during moderate activity. Consequently, T01 may outperform T04, which could be more tailored to storm-specific dynamics that are not prominent in this dataset.

Finally, in Figures 8 (upper panel) and 9, we present the magnetic field dynamics along an artificial circular polar orbit during storm and non-storm period, respectively. The field is calculated using the most accurate model for this analysis, the T01 model. This orbit is created artificially as a circular polar orbit with a radius of approximately 7 RE, which closely resembles the orbit of the MAAX satellite. Since the polar satellite observed only 3,435.85 hours out of the total 8,760 hours in the high-latitude, high-altitude polar cap (60 latitude) and auroral zone magnetic field, MAAX, equipped with an in situ magnetometer, will enhance the development of more accurate magnetospheric models and improve magnetic field mapping from ionospheric foot points to spacecraft in the equatorial plane.

In summary, we utilized a one-year dataset (1997) of Polar magnetometer (MFE) observations to analyze the spatial distribution of the magnetic field along its highly elliptical orbit. To obtain the external magnetic field, we subtracted Earth's internal magnetic field estimated using the IGRF-95 from the observed field. Additionally, we employed four widely used magnetospheric magnetic field modelsT89, T96, T01, and T04to calculate the magnetic field along the satellite's orbit, incorporating concurrent solar wind parameters, IMF By/Bz, and the Dst index as inputs. We then compared the observed external magnetic field with the modeled fields through scatter plots, spatial distribution analyses, and differences between the observed and modeled magnetic fields. The purpose of this comparison is to identify which of the four magnetic field models provides the most accurate predictions of the field observed by the Polar magnetometer. Our analysis revealed that the T01 model aligns most closely with the observed data, outperforming the other three models, including the more advanced T04 model, for the datasets and study period considered. Subsequently, we designed a circular polar orbit with a radius of 7 RE, which will be identical to the proposed MAAX mission trajectory. Finally, we calculated the magnetic field distribution along this circular polar orbit for the same study period. The results suggest that the magnetic field along the circular polar orbit will closely align with the predictions made by the T01 model for these conditions, demonstrating its ability in approximating the magnetic field distribution for a circular orbit similar to the proposed MAAX mission. These findings are valuable for future mission planning, as they demonstrate the potential of the T01 model (among the T89, T96 and T04 models) to predict external magnetic field variations accurately in a circular orbital configuration, aiding in mission design and data interpretation.

5 Open Research

All the data used in this study (Polar) are accessible via the NASA Space Physics Data Facility (SPDF) at `cdaweb.gsfc.nasa.gov/pub/data`, the OMNI dataset (https://omniweb.gsfc.nasa.gov/), the SpacePy Python package (https://spacepy.github.io/index.html), and the Geopack Python library (https://github.com/tsssss/geopack).

Acknowledgments

The authors wish to thank Guan Le at NASA/Goddard Space Flight Center who gave us valuable comments on this study. This work was partially supported by NASA Grant 80GSFC23CA042 and 80NSSC20K1779.

This article is protected by copyright. All rights reserved.

Author Manuscript

References

Brito, T. V., & Morley, S. K. (2017, December). Improving Empirical Magnetic Field Models by Fitting to In Situ Data Using an Optimized Parameter Approach. *Space Weather*, *15*(12), 1628–1648. Retrieved 2025-02-22, from https://agupubs.onlinelibrary.wiley.com/doi/10.1002/2017SW001702 doi: 10.1002/2017SW001702

Fairfield, D. H., Acuna, M. H., Zanetti, L. J., & Potemra, T. A. (1987, July). The magnetic field of the equatorial magnetotail: AMPTE/CCE observations at R < 8.8 R_e. *Journal of Geophysical Research: Space Physics*, *92*(A7), 7432–7442. Retrieved 2025-01-17, from https://agupubs.onlinelibrary.wiley.com/doi/10.1029/JA092iA07p07432 doi: 10.1029/JA092iA07p07432

Ganushkina, N. Y., Liemohn, M. W., & Dubyagin, S. (2018). Current Systems in the Earth's Magnetosphere. *Reviews of Geophysics*, *56*(2), 309–332. Retrieved 2023-01-19, from https://onlinelibrary.wiley.com/doi/abs/10.1002/2017RG000590 (_eprint: https://onlinelibrary.wiley.com/doi/pdf/10.1002/2017RG000590) doi: 10.1002/2017RG000590

Ganushkina, N. Y., Liemohn, M. W., Dubyagin, S., Daglis, I. A., Dandouras, I., De Zeeuw, D. L., ... Amariutei, O. (2015, November). Defining and resolving current systems in geospace. *Annales Geophysicae*, *33*(11), 1369–1402. Retrieved 2025-01-17, from https://angeo.copernicus.org/articles/33/1369/2015/ doi: 10.5194/angeo-33-1369-2015

Glatzmaiers, G. A., & Roberts, P. H. (1995, September). A three-dimensional self-consistent computer simulation of a geomagnetic field reversal. *Nature*, *377*(6546), 203–209. Retrieved 2025-01-17, from https://www.nature.com/articles/377203a0 doi: 10.1038/377203a0

Hoffmann, A. P., & Moldwin, M. B. (2024, December). *In Situ Calculation of Spaceflight Magnetometer Coupling Coefficients for Interference Removal using the Reduction Algorithm for Magnetometer Electromagnetic Noise (RAMEN).* Retrieved 2025-02-21, from https://essopenarchive.org/users/525947/articles/1214318-in-situ-calculation-of-spaceflight-magnetometer-coupling-coefficients-for-interference-removal-using-the-reduction-algorithm-for-magnetometer-electromagnetic-noise-ramen?commit=425fb17b555b3680e33c257994ef3199e0727109 doi: 10.22541/essoar.173445309.90631035/v1

Iijima, T., Potemra, T. A., & Zanetti, L. J. (1990). Large-scale characteristics of magnetospheric equatorial currents. *J. Geophys. Res.*, *95*, 991–999.

King, J. H. (2005). Solar wind spatial scales in and comparisons of hourly Wind and ACE plasma and magnetic field data. *Journal of Geophysical Research*, *110*(A2), 2104.

Le, G., & Russell, C. T. (1998, August). Initial Polar magnetic field experiment observations of the lowaltitude polar magnetosphere: Monitoring the ring current with polar orbiting spacecraft. *Journal of Geophysical Research: Space Physics*, *103*(A8), 17345–17350. Retrieved 2025-01-20, from https://agupubs.onlinelibrary.wiley.com/doi/10.1029/97JA02876 doi: 10.1029/97JA02876

Mead, G. D., & Fairfield, D. H. (1975, February). A quantitative magnetospheric model derived from spacecraft magnetometer data. *Journal of Geophysical Research*, *80*(4), 523–534. Retrieved 2025-01-17, from http://doi.wiley.com/10.1029/JA080i004p00523 doi: 10.1029/JA080i004p00523

Nakabe, S., Iyemori, T., Sugiura, M., & Slavin, J. A. (1997, August). A statistical study of the magnetic field structure in the inner magnetosphere. *Journal of Geophysical Research: Space Physics*, *102*(A8), 17571–17582. Retrieved 2025-01-17, from https://agupubs.onlinelibrary.wiley.com/doi/10.1029/97JA01181 doi: 10.1029/97JA01181

This article is protected by copyright. All rights reserved.

Author Manuscript

Nishimura, Y., Bortnik, J., Li, W., Thorne, R. M., Lyons, L. R., Angelopoulos, V., ... Auster, U. (2011, July). Estimation of magnetic field mapping accuracy using the pulsating aurora-chorus connection: MAGNETIC MAPPING WITH CHORUS AND AURORA. *Geophysical Research Letters*, *38*(14), n/a–n/a. Retrieved 2025-01-26, from http://doi.wiley.com/10.1029/2011GL048281 doi: 10.1029/2011GL048281

Olson, W. P., & Pfitzer, K. A. (1974, September). A quantitative model of the magnetospheric magnetic field. *Journal of Geophysical Research*, *79*(25), 3739–3748. Retrieved 2025-01-17, from http://doi.wiley.com/10.1029/JA079i025p03739 doi: 10.1029/JA079i025p03739

Qin, Z., Denton, R. E., Tsyganenko, N. A., & Wolf, S. (2007, November). Solar wind parameters for magnetospheric magnetic field modeling. *Space Weather*, *5*(11), 2006SW000296. Retrieved 2025-01-25, from https://agupubs.onlinelibrary.wiley.com/doi/10.1029/2006SW000296 doi: 10.1029/2006SW000296

Regoli, L. H., Moldwin, M. B., Pellioni, M., Bronner, B., Hite, K., Sheinker, A., & Ponder, B. M. (2018, March). Investigation of a low-cost magneto-inductive magnetometer for space science applications. *Geoscientific Instrumentation, Methods and Data Systems*, *7*(1), 129–142. Retrieved 2025-02-21, from https://gi.copernicus.org/articles/7/129/2018/ doi: 10.5194/gi-7-129-2018

Russell, C. T., Snare, R. C., Means, J. D., Pierce, D., Dearborn, D., Larson, M., ... Le, G. (1995). The GGS/POLAR magnetic fields investigations. *Space Sci. Rev.*, *71*, 563–582.

Sugiura, M., Ledley, B. G., Skillman, T. L., & Heppner, J. P. (1971, November). Magnetospheric-field distortions observed by Ogo 3 and 5. *Journal of Geophysical Research*, *76*(31), 7552–7565. Retrieved 2025-01-17, from http://doi.wiley.com/10.1029/JA076i031p07552 doi: 10.1029/JA076i031p07552

Tsyganenko, N. (1996). Effects of the solar wind conditions on the global magnetospheric configuration as deduced from data-based field models.. Retrieved from https://api.semanticscholar.org/CorpusID:117799460

Tsyganenko, N. A. (1989). A Magnetospheric Magnetic Field Model with a Warped Tail Current Sheet. *Planet. Space Sci.*, *37*, 5.

Tsyganenko, N. A. (1999, May). A study of the inner magnetosphere based on data of Polar. *Journal of Geophysical Research: Space Physics*, *104*(A5), 10275–10283. Retrieved 2025-02-20, from https://agupubs.onlinelibrary.wiley.com/doi/10.1029/1998JA900160 doi: 10.1029/1998JA900160

Tsyganenko, N. A. (2002a). A model of the near magnetosphere with a dawn-dusk asymmetry - 1. Mathematical Structure. *J. Geophys. Res.*, *107*, 10.1029/2001JA000219.

Tsyganenko, N. A. (2002b, August). A model of the near magnetosphere with a dawndusk asymmetry 1. Mathematical structure. *Journal of Geophysical Research: Space Physics*, *107*(A8). Retrieved 2025-01-25, from https://agupubs.onlinelibrary.wiley.com/doi/10.1029/2001JA000219 doi: 10.1029/2001JA000219

Tsyganenko, N. A., & Sitnov, M. I. (2005, March). Modeling the dynamics of the inner magnetosphere during strong geomagnetic storms. *Journal of Geophysical Research (Space Physics)*, *110*, A03208. doi: 10.1029/2004JA010798

Zhou, X., Russell, C. T., Le, G., & Tsyganenko, N. (1997, June). Comparison of observed and model magnetic fields at high altitudes above the polar cap: POLAR initial results. *Geophysical Research Letters*, *24*(12), 1451–1454. Retrieved 2025-01-20, from https://agupubs.onlinelibrary.wiley.com/doi/10.1029/97GL01406 doi: 10.1029/97GL01406

This article is protected by copyright. All rights reserved.